

# DNF-Intrinsic: Deterministic Noise-Free Diffusion for Indoor Inverse Rendering

Rongjia Zheng<sup>1</sup> Qing Zhang<sup>1,3\*</sup> Chengjiang Long<sup>2</sup> Wei-Shi Zheng<sup>1,3</sup>

<sup>1</sup> Sun Yat-sen University, China <sup>2</sup> Meta Reality Labs, USA

<sup>3</sup> Key Laboratory of Machine Intelligence and Advanced Computing, Ministry of Education, China

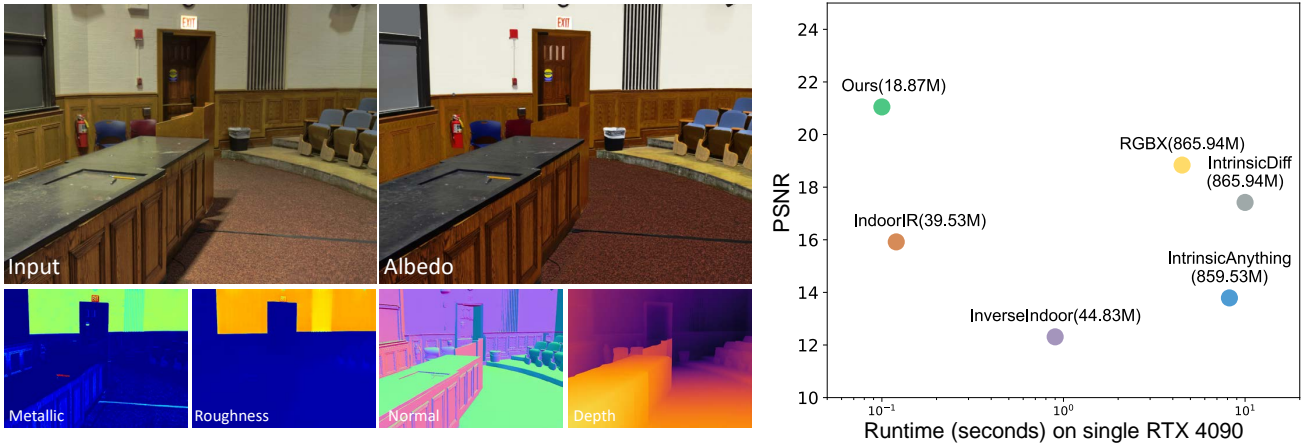


Figure 1. **Performance of our method on indoor inverse rendering.** By fine-tuning a pre-trained diffusion model on InteriorVerse [61], a synthetic indoor scene dataset, we achieve state-of-the-art indoor inverse rendering that can robustly recover albedo, metallic, roughness, normal, and depth from a single RGB indoor image. Taking albedo estimation as an example, as shown on the right, our method not only obtains significantly better results (21.05 in PSNR) than existing methods, *e.g.*, InverseIndoor [32], IndoorIR [61], IntrinsicAnything [13], IntrinsicDiff [28], and RGBX [58], but also enjoys the fastest inference speed (0.1 seconds with a single step) and fewest trainable parameters (18.87M). Note, the PSNR and runtime performance on the right are evaluated on the test set of the InteriorVerse dataset.

## Abstract

Recent methods have shown that pre-trained diffusion models can be fine-tuned to enable generative inverse rendering by learning image-conditioned noise-to-intrinsic mapping. Despite their remarkable progress, they struggle to robustly produce high-quality results as the noise-to-intrinsic paradigm essentially utilizes noisy images with deteriorated structure and appearance for intrinsic prediction, while it is common knowledge that structure and appearance information in an image are crucial for inverse rendering. To address this issue, we present DNF-Intrinsic, a robust yet efficient inverse rendering approach fine-tuned from a pre-trained diffusion model, where we propose to take the source image rather than Gaussian noise as input to directly predict deterministic intrinsic properties via flow matching. Moreover, we design a generative renderer to constrain that the predicted intrinsic properties are physically faithful to the source image. Experiments on both synthetic and real-world datasets show that our method clearly outperforms existing state-of-the-art methods. Our code is available at

<https://github.com/OnlyZZZZ/DNF-Intrinsic>.

## 1. Introduction

Inverse rendering has long been a fundamental task in computer vision and graphics since originated by Barrow and Tenenbaum [5]. It aims to reverse the rendering process by estimating the scene material (*e.g.*, albedo, metallic, and roughness), geometry (*e.g.*, normal and depth), and lighting from a single image. This task was widely studied as acquiring these intrinsic properties allows a wide range of applications including AR/VR [37], segmentation and tracking [6, 44], relighting and material editing [57], as well as robotics and autonomous driving [12].

Currently, inverse rendering remains a challenging open problem due to the following reasons. First, the problem is highly ill-posed, especially when only a single image with complex appearance effects (*e.g.*, inter-reflection and cast shadows) is given. Second, there is a lack of large-scale real-world datasets with ground-truth intrinsic properties in this field, which makes it difficult to achieve inverse rendering of real-world scenes in a data-driven manner.

\*Corresponding author.

Early methods often resort to hand-crafted priors to reduce the ambiguity of the problem [3, 4, 22]. However, as these priors do not always hold in real-world images, they may not work well for complex scenes. Benefiting from the emergence of large-scale synthetic datasets [33, 51, 61], learning-based methods [18, 31, 32, 34–36, 61, 62] casting inverse rendering as fully supervised image-to-image translation later became mainstream, but they often do not generalize well to real-world images.

A recent trend that has received considerable attention is to leverage the strong image prior of pre-trained diffusion models to achieve non-deterministic inverse rendering in a generative noise-to-intrinsic fashion. Following this paradigm, some methods propose to tackle inverse rendering by fine-tuning pre-trained diffusion models using synthetic data [13, 28, 41, 58]. However, they basically have the following three limitations. First, they cannot robustly produce high-quality results because the use of noise-to-intrinsic paradigm makes it impossible for them to exploit the complete image structure and appearance information for intrinsic prediction. Second, their inference speed is generally low, as a large number of denoising steps are usually required to map random noise to intrinsic properties. Finally, due to the lack of explicit constraint on image reconstruction from the predicted intrinsic properties, they may fail to achieve physically convincing inverse rendering.

To address these limitations, we present DNF-Intrinsic, a diffusion-based inverse rendering approach that allows for robust, efficient, and physically convincing single-image inverse rendering of indoor scenes (see Figure 1). Instead of learning image-conditioned noise-to-intrinsic mapping like previous methods, we advocate for image-to-intrinsic mapping<sup>1</sup>, where we take the source image rather than Gaussian noise as input to predict intrinsic properties in a deterministic manner using flow matching. This not only allows our method to obtain better intrinsic prediction performance by taking full advantage of the visual information in the source image, but also helps avoid the high computational cost arising from a large number of denoising steps. A generative renderer is further designed to achieve physically meaningful inverse rendering by explicitly constraining that the source image can be reconstructed from the predicted intrinsic properties. In summary, our main contributions are:

- We present a deterministic noise-free diffusion-based approach that enables robust yet efficient single-image inverse rendering of indoor scenes.
- We show that image-to-intrinsic mapping rather than image-conditioned noise-to-intrinsic mapping is a more effective choice for diffusion-based inverse rendering. Besides, we design a generative renderer to

<sup>1</sup>As verified by [2, 42] and our experiments, the prior in pre-trained diffusion model still holds when the model is fine-tuned with noise-free image-to-target mapping.

constrain the predicted intrinsic properties to be physically more reliable.

- Extensive experiments show that our method significantly outperforms state-of-the-art approaches on both synthetic and real-world datasets.

## 2. Related Work

**Optimization/learning-based approaches.** Early works in this field focus on tackling intrinsic image decomposition (IID), a sub-problem of inverse rendering that aims to separate an image into reflectance and shading. Conventional IID methods mainly work by formulating optimization based on hand-crafted priors [3, 22], while subsequent IID methods are mostly learning-based [9–11, 16, 17, 60], due to the availability of various datasets [7, 29]. In addition to IID, other sub-tasks of inverse rendering such as material/lighting estimation [24, 30] and geometry (*e.g.*, depth and normal) prediction [1, 54, 55] also receive considerable research attention. However, these methods can only estimate one or two of the intrinsic properties. Although there are inverse rendering methods that enable joint estimation of several intrinsic properties, they are mostly tailored for single object [15, 19, 52] or require multi-view images as input [8, 36, 43]. By training on large-scale synthetic datasets [33, 47, 49, 61], several works achieve single-image inverse rendering of indoor scenes [32, 35, 49, 53, 61, 62], but their performance may severely deteriorate on real-world images due to the inherent domain gap issue.

**Diffusion-based approaches.** A recent research trend in this field is to leverage the powerful image prior learned by pre-trained diffusion models for tasks including geometry prediction [23, 27], material estimation [28], and inverse rendering [13, 41, 58]. However, these methods mostly adopt a similar image-conditioned noise-to-target paradigm, which is highly sensitive to random noise initialization and introduces undesirable detail distortions. As shown by Tables 1 and 2 as well as Figure 4, they fail to enable robust performance and typically correspond to low inference speed due to the requirement of a large number of diffusion denoising steps (see Figures 1 and 8).

## 3. Method

Given a single RGB indoor image, the goal of our method is to recover its multiple intrinsic properties including albedo, metallic, roughness, normal, and depth via a single model fine-tuned from a pre-trained diffusion model. Figure 2 shows the overview of our method.

### 3.1. Problem Formulation

Unlike text-to-image generation, inverse rendering is a deterministic image-to-image task. To leverage the powerful diffusion prior, most previous diffusion-based inverse

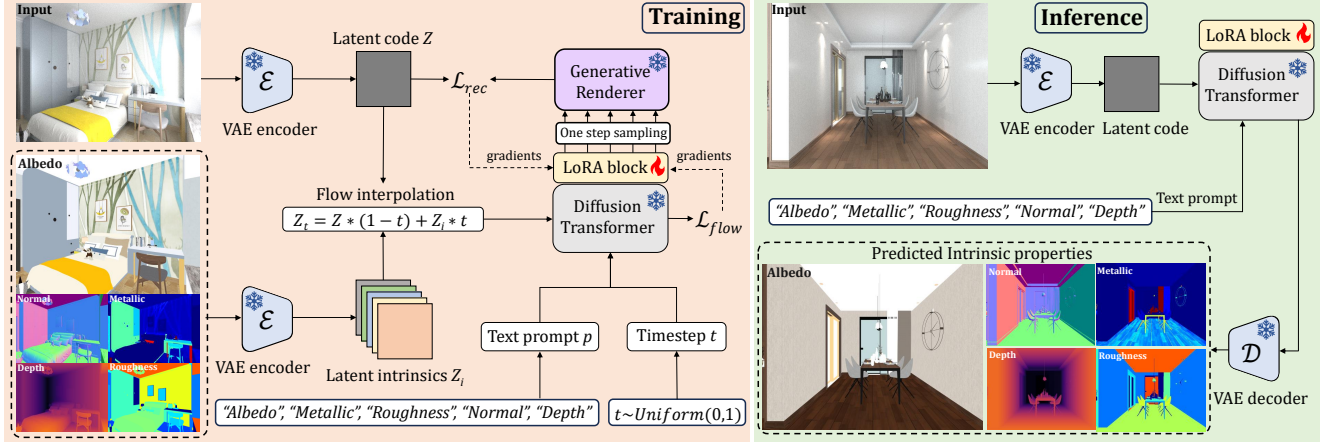


Figure 2. **Overview of our method.** Given a single indoor image, we aim to recover albedo, metallic, roughness, normal, and depth by learning deterministic image-to-intrinsic mappings triggered by text prompts. During training, instead of starting from noise as done in previous diffusion-based methods, we employ a pre-trained VAE encoder  $\mathcal{E}$  to initialize the latent code  $Z$  of the input image as the starting point of the flow trajectory. Then, the noised latent  $Z_t$  at timestep  $t$  is obtained by interpolation between  $Z$  and the latent intrinsic  $Z_i$ . Supervised by  $\mathcal{L}_{flow}$ , each noise latent and the corresponding text prompt are sent into a pre-trained diffusion transformer (DiT) with a trainable LoRA block to predict the flow velocity toward each intrinsic space. In addition, based on the one step sampling of all intrinsic properties, we develop a generative renderer to accordingly design a reconstruction loss  $\mathcal{L}_{rec}$  to provide supervision from the input image. During inference, starting from the latent code  $Z$ , we traverse each intrinsic flow triggered by its corresponding text prompt to obtain the predicted latent intrinsic and recover the final intrinsic properties using a VAE decoder  $\mathcal{D}$ .

rendering methods choose to follow text-to-image methods that formulate the task as a noise-to-intrinsic denoising diffusion problem conditioned on the input image. Taking albedo estimation as an example, the pre-trained diffusion model is usually trained to learn the conditional distribution  $D(A|I)$  over albedo  $A \sim \mathbb{R}^{W \times H \times 3}$ , where the condition  $I \sim \mathbb{R}^{W \times H \times 3}$  is an input image. The training objective of the diffusion model  $\epsilon_\theta$  is formulated as:

$$x_t = \sqrt{\bar{\alpha}_t}A + \sqrt{1 - \bar{\alpha}_t}\epsilon, t \in \{0, 1, \dots, T\}, \quad (1)$$

$$\mathcal{L} = \mathbb{E}_{t, A, \epsilon} \|\epsilon_\theta(x_t, t, I) - \epsilon\|_2^2, \quad (2)$$

where  $\bar{\alpha}_t$  refers to noise schedule,  $x_t$  is the noised image at timestep  $t$  and  $\epsilon \sim \mathcal{N}(0, \mathbf{I})$  represents Gaussian noise. Next, the backward denoising process gradually remove the noise in  $x_t$  to get  $x_{t-1}$ :

$$d(x_t) = \sqrt{1 - \bar{\alpha}_{t-1}} - \tau^2 \epsilon_\theta, \quad (3)$$

$$x_{t-1} = \sqrt{\bar{\alpha}_{t-1}} \left( \frac{x_t - \sqrt{1 - \bar{\alpha}_t} \epsilon_\theta}{\sqrt{\bar{\alpha}_t}} \right) + d(x_t) + \tau \epsilon, \quad (4)$$

where  $\tau$  is a parameter to control the amount of injected noise, and  $\epsilon_\theta = \epsilon_\theta(x_t, t, I)$  is the predicted noise. During inference, it starts with a pure Gaussian noise image  $x_T$  and gradually remove noise from  $t \in \{T \dots, 1, 0\}$  via Eq. (4), eventually leading to a clean albedo prediction.

**Our motivation.** Although the aforementioned image-conditioned noise-to-intrinsic paradigm has demonstrated

promising results on material [13, 28, 41, 58] and geometry estimation [23, 27, 56], there are still several issues to be addressed. First of all, this paradigm learns to operate on noisy images with deteriorated structure and appearance, which inevitably harms the overall performance as structure and appearance information are known to be crucial for inverse rendering [4, 14, 21]. Second, the inference speed of this paradigm is mostly low due to the inherent difficulty of mapping noise to target and the curved sampling trajectory defined by Eq. (4). Third, methods following this paradigm struggle to produce physically plausible high-quality intrinsic properties because they are often trained without explicitly enforcing that the predicted intrinsic properties are able to reconstruct the input image. The existence of the above issues motivates us to develop a diffusion-based inverse rendering method that learns image-to-intrinsic mapping taking the source image as input to predict reconstruction-constrained high-quality intrinsic properties in a deterministic and more efficient manner.

### 3.2. Deterministic Image-to-Intrinsic Diffusion

To enable more robust and efficient inverse rendering, we propose to learn a deterministic image-to-intrinsic mapping via flow matching [38, 39], rather than DDPM [25] based image-conditioned noise-to-intrinsic mapping like previous methods. Specifically, we use an ordinary differential equation (ODE) model to transfer the latent code of input image  $Z \sim \pi_I$  to the target latent intrinsic  $Z_p \sim \pi_p$  via a short

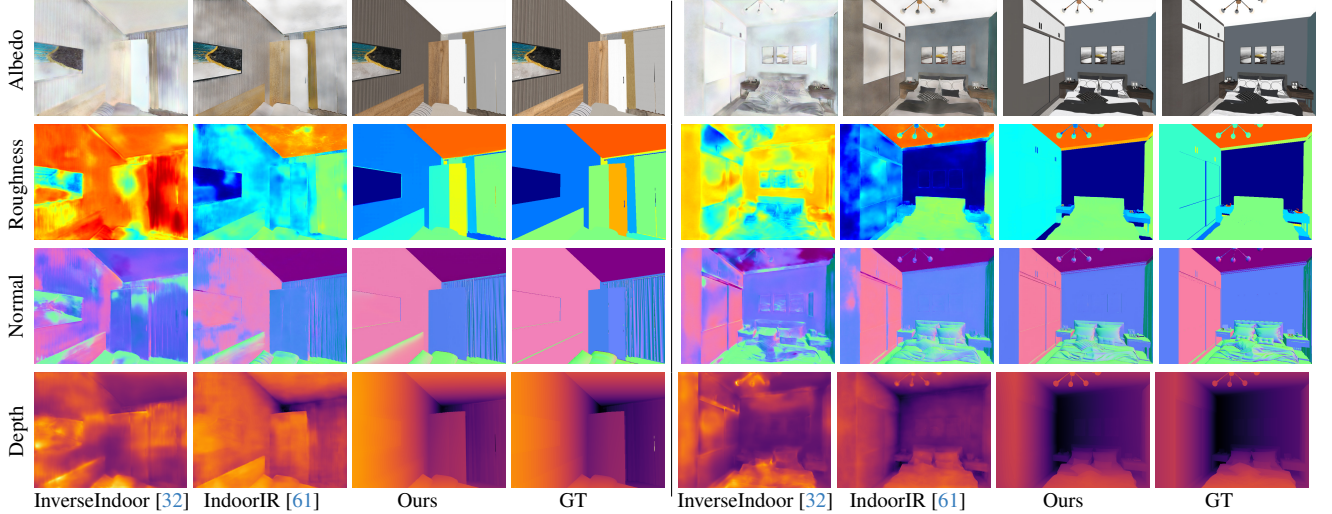


Figure 3. **Qualitative comparison of inverse rendering on the synthetic InteriorVerse dataset [61].** Although both our method and IndoorIR [61] enable metallic estimation, we here do not compare on metallic as InverseIndoor [32] cannot predict it. Please see the supplementary material for more results and comparison on metallic estimation.

and straight trajectory, enabling prediction with only a small number of sampling steps. During training, the noised latent  $Z_t$  is obtained by interpolation:

$$Z_t = Z * (1 - t) + Z_p * t, t \in [0, 1], \quad (5)$$

where  $t \in [0, 1]$  is a normalized timestep. Then, a neural network  $\mu_\theta$  is employed to learn the flow velocity along the path between the input image and each single intrinsic property using the loss below:

$$\mathcal{L}_{single} = \mathbb{E}_{t, Z, Z_p} \|\mu_\theta(Z_t, t) - (Z_p - Z)\|_2^2. \quad (6)$$

In contrast to most previous methods that typically focus on the estimation of single or very limited number of intrinsic properties, we aim to achieve holistic inverse rendering that jointly estimates five intrinsic properties. To this end, we use the text prompt of each intrinsic property as a trigger to adapt a single pre-trained diffusion model for prediction of multiple intrinsic properties, without modifying its architecture. Specifically, we formulate inverse rendering as a deterministic one-to-many distribution mapping problem, starting from the same latent code  $Z$  and diverging along different intrinsic trajectories towards various latent intrinsics  $Z_i$ . Hence, we use the text prompt as a simple trigger [58] to control the direction of the intrinsic trajectories. The training objective is defined as:

$$\mathcal{L}_{flow} = \mathbb{E}_{t, Z, Z_i} \sum_{i=1}^N \|\mu_\theta(Z_t, t, p_i) - (Z_i - Z)\|_2^2, \quad (7)$$

where  $N$  is the number of intrinsic types,  $p_i \in \{\text{“albedo”}, \text{“metallic”}, \text{“roughness”}, \text{“normal”}, \text{“depth”}\}$  refers to the

text trigger representing the target intrinsic property, while  $Z_i$  is the corresponding latent intrinsic.

Note, unlike previous methods that mostly use UNet for diffusion denoising, we experimentally found that Diffusion Transformer (DiT) [45] is a more effective flow estimator, as its utilization of global information is crucial to the success of inverse rendering. Hence, a pre-trained DiT from Stable Diffusion V3 [20] is fine-tuned to serve as our flow estimator  $\mu_\theta$ . Instead of fine-tuning the entire pre-trained model or adding extra ControlNet branches [59], we retain the original architecture of the pre-trained DiT and apply LoRA [26] to fine-tune a very small number of parameters.

### 3.3. Generative Renderer

Although each intrinsic property is supervised by the corresponding ground truth in the training dataset, there is actually no direct constraint between these properties and the input image, neglecting their potential relationship. To address this issue, we develop a generative renderer and accordingly design a reconstruction loss to ensure that we are able to reconstruct the input image from the predicted intrinsic properties. Specifically, we use ControlNet [59] to incorporate the five intrinsic properties as the control signal to a pre-trained model from Stable Diffusion [48] and fine-tune it as the generative renderer  $\mathcal{R}$  to render the input image based on the given ground-truth intrinsic properties:

$$x_t = \sqrt{\alpha_t}Z + \sqrt{1 - \alpha_t}\epsilon, t \in \{0, 1, \dots, T\}, \quad (8)$$

$$\mathcal{L} = \mathbb{E}_{t, Z, \epsilon} \|\mathcal{R}_\theta(x_t, t, (A, M, R, N, D)) - \epsilon\|_2^2, \quad (9)$$

where  $Z$  is the latent code of the input image and the condition signal is the combination of the five intrinsic prop-

Method	Albedo			Metallic			Roughness			Normal	Depth
	PSNR $\uparrow$	SSIM $\uparrow$	LPIPS $\downarrow$	PSNR $\uparrow$	SSIM $\uparrow$	LPIPS $\downarrow$	PSNR $\uparrow$	SSIM $\uparrow$	LPIPS $\downarrow$	AE $\downarrow$	AMRE $\downarrow$
InverseIndoor [32]	12.31	0.68	0.52	-	-	-	11.76	0.53	0.45	26.07	0.25
IndoorIR [61]	15.92	0.78	0.34	16.72	0.60	0.27	16.13	0.68	0.29	15.41	0.13
IntrinsicAnything [13]	13.79	0.67	0.36	-	-	-	-	-	-	-	-
IntrinsicDiff [28]	17.42	0.80	0.22	16.46	0.50	0.29	13.33	0.57	0.34	-	-
RGBX [58]	18.84	0.81	0.18	11.92	0.30	0.41	11.67	0.51	0.43	18.57	-
Ours	<b>21.95</b>	<b>0.87</b>	<b>0.12</b>	<b>17.64</b>	<b>0.63</b>	<b>0.22</b>	<b>16.72</b>	<b>0.71</b>	<b>0.24</b>	<b>12.23</b>	<b>0.08</b>

Table 1. **Quantitative comparison of inverse rendering on the synthetic InteriorVerse dataset [61].** Note, “-” means that the prediction of a certain intrinsic property is not allowed by a method.

erties including albedo ( $A$ ), metallic ( $M$ ), roughness ( $R$ ), normal ( $N$ ) and depth ( $D$ ). As the scene lighting is not provided as a conditioning input, we instead model the rendering process as property-conditioned noise-to-image mapping with stochasticity (*i.e.*, Gaussian noise) representing the unknown lighting conditions. Specifically, the pre-trained generative renderer  $\mathcal{R}$  is employed to formulate the following reconstruction loss:

$$\mathcal{L}_{rec} = \mathbb{E}_{t, Z, \epsilon} \left\| \mathcal{R}(\sqrt{\alpha_t}Z + \sqrt{1 - \alpha_t}\epsilon_t, t, \mu_\theta(I)) - \epsilon \right\|_2^2, \quad (10)$$

where  $\mu_\theta(I) = (\tilde{A}, \tilde{M}, \tilde{R}, \tilde{N}, \tilde{D})$  refers to one-step estimation of all five intrinsic properties while  $\epsilon_t$  is a sampled noise denoting the unknown lighting. Inspired by DreamFusion [46],  $\mathcal{L}_{rec}$  is implemented as the Score Distillation Sampling (SDS) loss to compute the gradient for  $\mu_\theta$  without backpropagating through the generative renderer  $\mathcal{R}$ . Specifically, we compute the gradient of  $\mathcal{L} = \mu_\theta(I) \cdot \text{stop\_gradient}[\mathcal{L}_{rec}]$  with respect to the parameters  $\theta$ . Then, the parameters can be updated using an optimizer.

**Discussion.** Note, to remedy the lack of lighting in the reconstruction loss, we sample various different lighting in the training iterations, which is functionally equivalent to integrating all the possible lighting. Therefore, by minimizing the reconstruction loss, our model will be trained towards the direction of removing the effect of lighting and finally converges on lighting-independent intrinsic properties. Please see the supplementary material for more details about the generative renderer.

### 3.4. Inference

As shown in Figure 2, during inference, the VAE encoder  $\mathcal{E}$  encodes the input image  $I$  into the latent code  $Z$ . Then, the directions of intrinsic trajectory are determined by specific text prompt  $p$ . Starting from the initial point  $Z_0 = Z$  with the prompt  $p_i$ , we can gradually transition towards the target latent intrinsic by:

$$Z_{t+\frac{1}{K}} = Z_t + \frac{1}{K}\mu_\theta(Z_t, t, p_i), \quad (11)$$

where  $K$  denotes the total number of sampling steps, which is set as 10 in all our experiments.  $t \in \{0, \dots, K-1\}/K$

is the normalized timestep. After obtaining the target latent intrinsic, we utilize the VAE decoder  $\mathcal{D}$  to recover the corresponding intrinsic property.

### 3.5. Implementation details

We follow previous methods [28, 61] to train our model on the synthetic InteriorVerse dataset [61] for 100 epochs. The dataset contains ground truth for albedo, metallic, roughness, normal, and depth, having a total of 45,073 samples for training and 2,672 samples for testing. The encoder  $\mathcal{E}$  and decoder  $\mathcal{D}$  are from the pre-trained variational autoencoder (VAE) in Stable Diffusion V3 [20]. During training, we apply LoRA to fine-tune the attention layers in the pre-trained diffusion transformer using the AdmaW optimizer [40] with a learning rate of 1e-4 and a weight decay rate of 1e-2. The rank of LoRA layer is set as 64 and the weights are initialized using Gaussian distribution. Furthermore, to adapt to pre-trained VAE, we transform the input image and intrinsic properties to the range of  $[-1, 1]$ . For single-channel intrinsic properties, *e.g.*, metallic, roughness, and depth, we replicate them across three channels during training to simulate the RGB image and average the output across channels during inference to recover them.

## 4. Experiments

### 4.1. Evaluation Datasets and Metrics

We evaluate our method on several benchmark indoor datasets including the synthetic InteriorVerse dataset [61] and several benchmark real-world indoor datasets, *i.e.*, IIW [7], DIODE [51], and NYUv2 [50]. For quantitative evaluation of albedo, metallic, and roughness on ground-truth available synthetic datasets, we employ the commonly-used PSNR, SSIM, and LPIPS to evaluate the prediction accuracy. We follow DSINE [1] to assess normal estimation by calculating the mean angular error (AE) and use the Absolute Mean Relative Error (AMRE) introduced in [27] for monocular depth evaluation. Note, for the IIW dataset with relative human albedo annotations rather than albedo itself, we follow [7] to use Weighted Human Disagreement Rate (WHDR) to evaluate the performance of albedo prediction.

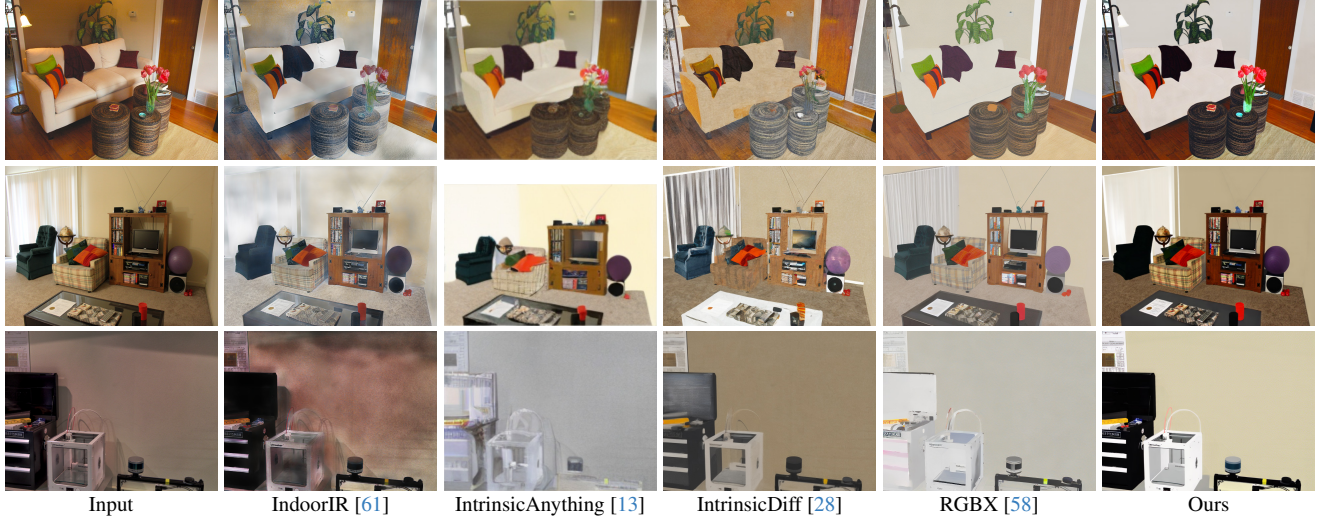


Figure 4. Qualitative comparison of albedo estimation on real-world images.

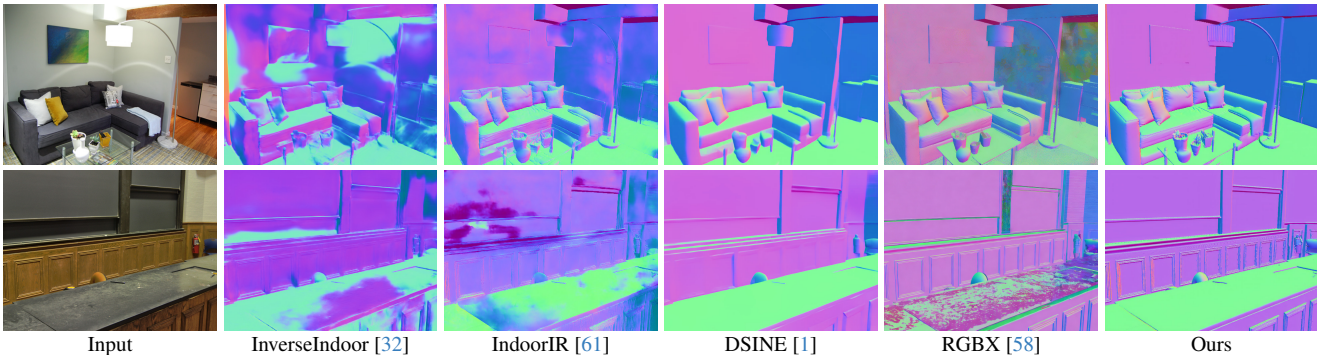


Figure 5. Qualitative comparison of normal estimation on real-world images.

Method	IIW		NYUv2		DIODE	
	WHDR↓	AE↓	AMRE↓	AE↓	AMRE↓	AMRE↓
InverseIndoor [32]	21.99	38.51	0.28	44.70	0.20	
IndoorIR [61]	22.90	34.38	0.23	36.03	0.19	
IntrinsicAnything [13]	27.75	-	-	-	-	
IntrinsicDiff [28]	22.02	-	-	-	-	
RGBX [58]	21.80	35.24	-	42.41	-	
Ours	<b>20.90</b>	<b>28.40</b>	<b>0.07</b>	<b>28.29</b>	<b>0.11</b>	

Table 2. Quantitative comparison of albedo and geometry estimation on real-world datasets. For fair comparison, all the methods here are not fine-tuned on these datasets.

## 4.2. Comparison with State-of-the-art Methods

**Baselines.** We compare our method with the following state-of-the-art methods: (i) two CNN-based inverse rendering methods, InverseIndoor [32] and IndoorIR [61], and (ii) three latest diffusion-based methods, IntrinsicDiff [28], IntrinsicAnything [13] and RGBX [58]. Note, we do not compare with other existing single-image inverse rendering

methods [35, 41, 49, 53, 62], as their codes and trained models are not publicly available. For fair comparisons, we produce results of the compared methods by fine-tuning their models on the InteriorVerse dataset [61].

**Evaluation on synthetic data.** Table 1 reports the quantitative comparison results of holistic inverse rendering on the synthetic InteriorVerse dataset. As shown, our method outperforms the compared methods on all five intrinsic properties. Figure 3 further presents visual comparison results, where we can see that our method robustly produces high-quality predictions closer to the ground truths while avoiding the common blurring or ghosting artifacts, demonstrating the effectiveness and robustness of our method.

**Evaluation on real-world data.** In addition to synthetic data, we also evaluate our method on real-world data. Specifically, we evaluate albedo estimation on the IIW dataset and conduct normal and depth comparisons on the NYUv2 and DIODE datasets. As shown in Table 2, our

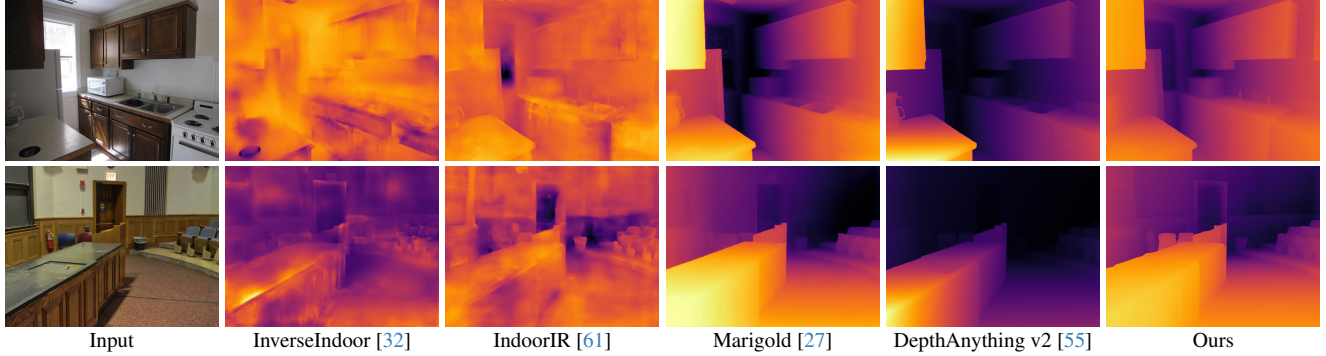


Figure 6. Qualitative comparison of depth estimation on real-world images.



Figure 7. Qualitative ablation study on real-world albedo estimation.

method exhibits a clear advantage over the compared methods on these real-world datasets. Figure 4 presents visual comparisons on albedo estimation, where we can see that our method produces albedo predictions that are more faithful to the input images. Visual comparisons on normal and depth estimation are given in Figures 5 and 6, respectively. As can be seen, despite that our method is fine-tuned on the synthetic InteriorVerse dataset with only 45K training images, it can produce very competitive normal and depth prediction results, which are comparable to current leading methods (basically trained on datasets significantly larger than ours) specifically designed for normal [1] and depth [27, 55] estimation. Please see the supplementary material for more results as well as comparisons on roughness and metallic estimation.

### 4.3. Ablation Study

**Effect of deterministic image-to-intrinsic mapping.** To examine the effectiveness of our image-to-intrinsic mapping design, we compare it with several alternative designs: (i) **Noise+Flow+LoRA**: image-conditioned noise-to-intrinsic mapping learned by flow matching while fine-

Method	Params	PSNR $\uparrow$	SSIM $\uparrow$	LPIPS $\downarrow$
SD3+Noise+Flow+LoRA	19M	18.25	0.73	0.22
SD3+Image+DDPM+LoRA	19M	17.62	0.81	0.18
UNet from scratch	100M	17.99	0.78	0.25
DiT from scratch	300M	18.80	0.81	0.17
UNet from SD2	13M	19.51	0.83	0.15
Ours with ControlNet	1000M	17.13	0.68	0.27
Ours fine-tuning all parameters	2047M	21.30	0.85	0.14
Ours w/o reconstruction loss $\mathcal{L}_{rec}$	19M	21.03	0.82	0.14
Ours (SD3+Image+Flow+LoRA)	19M	<b>21.95</b>	<b>0.87</b>	<b>0.12</b>

Table 3. Quantitative ablation study on albedo estimation on the InteriorVerse dataset [61].

tuning with LoRA. (ii) **Image+DDPM+LoRA**: image-to-intrinsic mapping using v-prediction of DDPM while fine-tuning with LoRA. As shown in Figure 7(b)-(c) and Table 3 (see 2nd and 3rd rows), our approach achieves better results than the alternatives, validating the superiority of our deterministic image-to-intrinsic mapping design.

**Effect of diffusion prior.** To evaluate the effectiveness of the pre-trained diffusion prior, we compare our method with two alternative models trained from scratch with UNet and

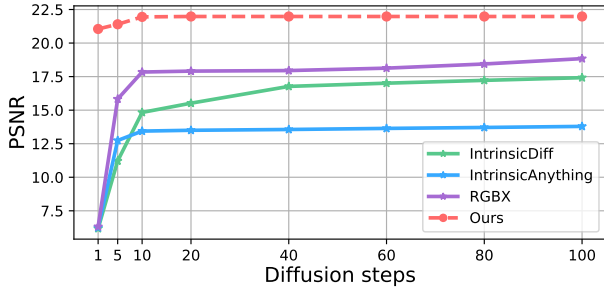


Figure 8. **Quantitative comparison of albedo estimation using varying diffusion steps on the InteriorVerse dataset.** In comparison to recent diffusion-based inverse rendering methods, *e.g.*, IntrinsicDiff [28], IntrinsicAnything [13], and RGBX [58], our method achieves better albedo estimation in fewer diffusion steps.

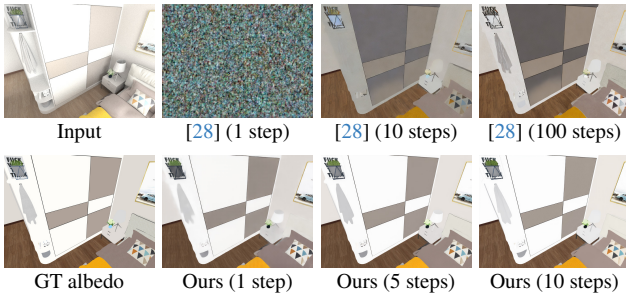


Figure 9. **Qualitative comparison of albedo estimation using different number of diffusion steps.**

diffusion transformer (DiT), respectively. As shown in Figure 7(d)-(e) and Table 3 (see 4th and 5th rows), despite having more trainable parameters, the two models trained from scratch fail to produce satisfactory results, verifying the effectiveness of the diffusion prior.

**Effect of Diffusion Transformer (DiT).** Figure 7(f) and the 6th row in Table 3 provide a comparison between UNet from Stable Diffusion v2 (SD2) and our utilized DiT from Stable Diffusion v3 (SD3). As shown, replacing DiT with UNet leads to an obvious performance drop.

**Effect of different fine-tuning strategies.** Figure 7(g)-(h) and Table 3 (see 7th and 8th rows) provide comparisons between fine-tuning with ControlNet, fine-tuning all parameters, and fine-tuning with LoRA (ours). As shown, our fine-tuning with LoRA strategy achieves the best performance while corresponding to the fewest trainable parameters.

**Effect of the reconstruction loss  $\mathcal{L}_{rec}$ .** As shown in the 9th row in Table 3, the reconstruction loss  $\mathcal{L}_{rec}$  is beneficial to obtain better results. Moreover, Figure 7(i) shows that omitting the loss would lead to an albedo prediction with clear shadow residuals on the wall.

**Effect of different number of diffusion steps.** We evaluate the performance of our method with different numbers



Figure 10. **Applications.** Our method allows to produce photorealistic object insertion, as well as lighting and material editing.

of diffusion steps in Figures 8 and 9. In contrast to the latest diffusion-based methods [13, 28, 58], our approach achieves superior results using significantly fewer steps.

#### 4.4. Applications

Thanks to the high-quality material and geometry properties recovered from a single image, our method enables various applications. As shown in Figure 23, our method can produce visually pleasing results for object insertion, lighting, and material editing. Note, although our method itself does not allow for lighting estimation because our training dataset does not provide ground-truth for lighting, we can estimate it via image reconstruction optimization. Specifically, we use pre-integrated environment lighting parameterized by Spherical Gaussians (SG) for global illumination, along with 48 SG emission profiles to represent point lights [28]. The SG parameters are then determined by optimizing a reconstruction loss between the re-rendered output and the input. With the estimated lighting, we can achieve controllable lighting editing and 3D object insertion.

#### 5. Conclusion

We have presented DNF-Intrinsic, a deterministic noise-free diffusion-based approach that allows for robust yet efficient single-image inverse rendering of indoor scenes. Unlike previous methods that learn image-conditioned noise-to-intrinsic mapping, we propose to take the source image rather than Gaussian noise as input to learn deterministic image-to-intrinsic mapping via flow matching. By this means, our method achieves more robust intrinsic prediction performance by taking full advantage of the visual information in the source image while avoiding the high computational cost from multiple denoising steps. A generative

renderer is also designed to ensure the resulting intrinsic properties are physically meaningful. Experiments show that our method outperforms previous approaches.

**Acknowledgement.** This work was supported by the National Natural Science Foundation of China (62471499), the Guangdong Basic and Applied Basic Research Foundation (2023A1515030002).

## References

- [1] Gwangbin Bae and Andrew J Davison. Rethinking inductive biases for surface normal estimation. In *CVPR*, 2024. 2, 5, 7
- [2] Arpit Bansal, Eitan Borgnia, Hong-Min Chu, Jie Li, Hamid Kazemi, Furong Huang, Micah Goldblum, Jonas Geiping, and Tom Goldstein. Cold diffusion: Inverting arbitrary image transforms without noise. *NeurIPS*, 36, 2023. 2
- [3] Jonathan T Barron and Jitendra Malik. Shape, albedo, and illumination from a single image of an unknown object. In *CVPR*, pages 334–341, 2012. 2
- [4] Jonathan T Barron and Jitendra Malik. Shape, illumination, and reflectance from shading. *IEEE Transactions on Pattern Analysis and Machine Intelligence*, 37(8):1670–1687, 2014. 2, 3
- [5] Harry Barrow, J Tenenbaum, A Hanson, and E Riseman. Recovering intrinsic scene characteristics. *Comput. vis. syst.*, 2(3-26):2, 1978. 1
- [6] Anil S Baslamisli, Thomas T Groenestege, Partha Das, Hoang-An Le, Sezer Karaoglu, and Theo Gevers. Joint learning of intrinsic images and semantic segmentation. In *ECCV*, pages 286–302, 2018. 1
- [7] Sean Bell, Kavita Bala, and Noah Snavely. Intrinsic images in the wild. *ACM Transactions on Graphics (TOG)*, 33(4):1–12, 2014. 2, 5
- [8] Mark Boss, Raphael Braun, Varun Jampani, Jonathan T Barron, Ce Liu, and Hendrik Lensch. Nerd: Neural reflectance decomposition from image collections. In *ICCV*, pages 12684–12694, 2021. 2
- [9] Chris Careaga and Yağız Aksoy. Intrinsic image decomposition via ordinal shading. *ACM Transactions on Graphics*, 43(1):1–24, 2023. 2
- [10] Chris Careaga and Yağız Aksoy. Colorful diffuse intrinsic image decomposition in the wild. *ACM Transactions on Graphics (TOG)*, 43(6):1–12, 2024.
- [11] Chris Careaga, S Mahdi H Miangoleh, and Yağız Aksoy. Intrinsic harmonization for illumination-aware image compositing. In *SIGGRAPH Asia 2023 Conference Papers*, 2023. 2
- [12] Arkadeep Narayan Chaudhury, Leonid Keselman, and Christopher G Atkeson. Shape from shading for robotic manipulation. In *WACV*, pages 8389–8398, 2024. 1
- [13] Xi Chen, Sida Peng, Dongchen Yang, Yuan Liu, Bowen Pan, Chengfei Lv, and Xiaowei Zhou. Intrinsicanything: Learning diffusion priors for inverse rendering under unknown illumination. In *ECCV*, 2024. 1, 2, 3, 5, 6, 8
- [14] Tianhang Cheng, Wei Chiu Ma, Kaiyu Guan, Antonio Torralba, and Shenlong Wang. Structure from duplicates: Neural inverse graphics from a pile of objects. *NeurIPS*, 36, 2023. 3
- [15] Hoon-Gyu Chung, Seokjun Choi, and Seung-Hwan Baek. Differentiable point-based inverse rendering. In *CVPR*, pages 4399–4409, 2024. 2
- [16] Partha Das, Sezer Karaoglu, and Theo Gevers. Pie-net: Photometric invariant edge guided network for intrinsic image decomposition. In *CVPR*, 2022. 2
- [17] Partha Das, Maxime Gevers, Sezer Karaoglu, and Theo Gevers. Idtransformer: Transformer for intrinsic image decomposition. In *ICCV*, pages 816–825, 2023. 2
- [18] Xiaodan Du, Nicholas Kolkin, Greg Shakhnarovich, and Anand Bhattad. Generative models: What do they know? do they know things? let’s find out! *arXiv preprint arXiv:2311.17137*, 2023. 2
- [19] Yuto Enyo and Ko Nishino. Diffusion reflectance map: Single-image stochastic inverse rendering of illumination and reflectance. In *CVPR*, pages 11873–11883, 2024. 2
- [20] Patrick Esser, Sumith Kulal, Andreas Blattmann, Rahim Entezari, Jonas Müller, Harry Saini, Yam Levi, Dominik Lorenz, Axel Sauer, Frederic Boesel, et al. Scaling rectified flow transformers for high-resolution image synthesis. In *ICML*, 2024. 4, 5
- [21] Qingnan Fan, Jiaolong Yang, Gang Hua, Baoquan Chen, and David Wipf. Revisiting deep intrinsic image decompositions. In *CVPR*, pages 8944–8952, 2018. 3
- [22] Graham D Finlayson, Mark S Drew, and Cheng Lu. Intrinsic images by entropy minimization. In *ECCV*, 2004. 2
- [23] Xiao Fu, Wei Yin, Mu Hu, Kaixuan Wang, Yuexin Ma, Ping Tan, Shaojie Shen, Dahua Lin, and Xiaoxiao Long. Geowizard: Unleashing the diffusion priors for 3d geometry estimation from a single image. In *ECCV*, 2024. 2, 3
- [24] Marc-André Gardner, Yannick Hold-Geoffroy, Kalyan Sunkavalli, Christian Gagné, and Jean-François Lalonde. Deep parametric indoor lighting estimation. In *ICCV*, pages 7175–7183, 2019. 2
- [25] Jonathan Ho, Ajay Jain, and Pieter Abbeel. Denoising diffusion probabilistic models. *NeurIPS*, 2020. 3
- [26] Edward J Hu, Yelong Shen, Phillip Wallis, Zeyuan Allen-Zhu, Yuanzhi Li, Shean Wang, Lu Wang, and Weizhu Chen. Lora: Low-rank adaptation of large language models. *arXiv preprint arXiv:2106.09685*, 2021. 4
- [27] Bingxin Ke, Anton Obukhov, Shengyu Huang, Nando Metzger, Rodrigo Caye Daudt, and Konrad Schindler. Repurposing diffusion-based image generators for monocular depth estimation. In *CVPR*, pages 9492–9502, 2024. 2, 3, 5, 7
- [28] Peter Kocsis, Vincent Sitzmann, and Matthias Nießner. Intrinsic image diffusion for single-view material estimation. In *CVPR*, 2024. 1, 2, 3, 5, 6, 8, 12
- [29] Balazs Kovacs, Sean Bell, Noah Snavely, and Kavita Bala. Shading annotations in the wild. In *CVPR*, 2017. 2
- [30] Chloe LeGendre, Wan-Chun Ma, Graham Fyffe, John Flynn, Laurent Charbonnel, Jay Busch, and Paul Debevec. Deep-light: Learning illumination for unconstrained mobile mixed reality. In *CVPR*, pages 5918–5928, 2019. 2
- [31] Chenhao Li, Trung Thanh Ngo, and Hajime Nagahara. Inverse rendering of translucent objects using physical and neural renderers. In *CVPR*, pages 12510–12520, 2023. 2

- [32] Zhengqin Li, Mohammad Shafiei, Ravi Ramamoorthi, Kalyan Sunkavalli, and Manmohan Chandraker. Inverse rendering for complex indoor scenes: Shape, spatially-varying lighting and svbrdf from a single image. In *CVPR*, pages 2475–2484, 2020. 1, 2, 4, 5, 6
- [33] Zhengqin Li, Ting-Wei Yu, Shen Sang, Sarah Wang, Meng Song, Yuhan Liu, Yu-Ying Yeh, Rui Zhu, Nitesh Gundavarapu, Jia Shi, et al. Openrooms: An end-to-end open framework for photorealistic indoor scene datasets. *arXiv preprint arXiv:2007.12868*, 2020. 2
- [34] Zhengqin Li, Jia Shi, Sai Bi, Rui Zhu, Kalyan Sunkavalli, Miloš Hašan, Zexiang Xu, Ravi Ramamoorthi, and Manmohan Chandraker. Physically-based editing of indoor scene lighting from a single image. In *ECCV*, pages 555–572. Springer, 2022. 2
- [35] Zhen Li, Lingli Wang, Xiang Huang, Cihui Pan, and Jiaqi Yang. Phyr: Physics-based inverse rendering for panoramic indoor images. In *CVPR*, pages 12713–12723, 2022. 2, 6
- [36] Zhen Li, Lingli Wang, Mofang Cheng, Cihui Pan, and Jiaqi Yang. Multi-view inverse rendering for large-scale real-world indoor scenes. In *CVPR*, 2023. 2
- [37] Ruofan Liang, Zan Gojcic, Merlin Nimier-David, David Acuna, Nandita Vijaykumar, Sanja Fidler, and Zian Wang. Photorealistic object insertion with diffusion-guided inverse rendering. *arXiv preprint arXiv:2408.09702*, 2024. 1
- [38] Yaron Lipman, Ricky TQ Chen, Heli Ben-Hamu, Maximilian Nickel, and Matt Le. Flow matching for generative modeling. *arXiv preprint arXiv:2210.02747*, 2022. 3
- [39] Xingchao Liu, Chengyue Gong, and Qiang Liu. Flow straight and fast: Learning to generate and transfer data with rectified flow. *arXiv preprint arXiv:2209.03003*, 2022. 3
- [40] I Loshchilov. Decoupled weight decay regularization. *arXiv preprint arXiv:1711.05101*, 2017. 5
- [41] Jundan Luo, Duygu Ceylan, Jae Shin Yoon, Nanxuan Zhao, Julien Philip, Anna Frühstück, Wenbin Li, Christian Richardt, and Tuanfeng Wang. Intrinsicdiffusion: Joint intrinsic layers from latent diffusion models. In *ACM SIGGRAPH 2024 Conference Papers*, 2024. 2, 3, 6
- [42] Gonzalo Martin Garcia, Karim Abou Zeid, Christian Schmidt, Daan de Geus, Alexander Hermans, and Bastian Leibe. Fine-tuning image-conditional diffusion models is easier than you think. In *WACV*, 2025. 2
- [43] Jacob Munkberg, Jon Hasselgren, Tianchang Shen, Jun Gao, Wenzheng Chen, Alex Evans, Thomas Müller, and Sanja Fidler. Extracting triangular 3d models, materials, and lighting from images. In *CVPR*, pages 8280–8290, 2022. 2
- [44] Julian Ost, Tanushree Banerjee, Mario Bijelic, and Felix Heide. Inverse neural rendering for explainable multi-object tracking. *arXiv preprint arXiv:2404.12359*, 2024. 1
- [45] William Peebles and Saining Xie. Scalable diffusion models with transformers. In *ICCV*, pages 4195–4205, 2023. 4
- [46] Ben Poole, Ajay Jain, Jonathan T Barron, and Ben Mildenhall. Dreamfusion: Text-to-3d using 2d diffusion. *arXiv preprint arXiv:2209.14988*, 2022. 5, 12
- [47] Mike Roberts, Jason Ramapuram, Anurag Ranjan, Atulit Kumar, Miguel Angel Bautista, Nathan Paczan, Russ Webb, and Joshua M Susskind. Hypersim: A photorealistic synthetic dataset for holistic indoor scene understanding. In *ICCV*, pages 10912–10922, 2021. 2
- [48] Robin Rombach, Andreas Blattmann, Dominik Lorenz, Patrick Esser, and Björn Ommer. High-resolution image synthesis with latent diffusion models. In *CVPR*, pages 10684–10695, 2022. 4
- [49] Soumyadip Sengupta, Jinwei Gu, Kihwan Kim, Guilin Liu, David W Jacobs, and Jan Kautz. Neural inverse rendering of an indoor scene from a single image. In *ICCV*, pages 8598–8607, 2019. 2, 6
- [50] Nathan Silberman, Derek Hoiem, Pushmeet Kohli, and Rob Fergus. Indoor segmentation and support inference from rgbd images. In *ECCV*, pages 746–760. Springer, 2012. 5
- [51] Igor Vasiljevic, Nick Kolkin, Shanyi Zhang, Ruotian Luo, Haochen Wang, Falcon Z Dai, Andrea F Daniele, Mohammadreza Mostajabi, Steven Basart, Matthew R Walter, et al. Diode: A dense indoor and outdoor depth dataset. *arXiv preprint arXiv:1908.00463*, 2019. 2, 5
- [52] Dor Verbin, Ben Mildenhall, Peter Hedman, Jonathan T Barron, Todd Zickler, and Pratul P Srinivasan. Eclipse: Disambiguating illumination and materials using unintended shadows. In *CVPR*, pages 77–86, 2024. 2
- [53] Zian Wang, Jonah Philion, Sanja Fidler, and Jan Kautz. Learning indoor inverse rendering with 3d spatially-varying lighting. In *ICCV*, pages 12538–12547, 2021. 2, 6
- [54] Lihe Yang, Bingyi Kang, Zilong Huang, Xiaogang Xu, Jiashi Feng, and Hengshuang Zhao. Depth anything: Unleashing the power of large-scale unlabeled data. In *CVPR*, 2024. 2
- [55] Lihe Yang, Bingyi Kang, Zilong Huang, Zhen Zhao, Xiaogang Xu, Jiashi Feng, and Hengshuang Zhao. Depth anything v2. *arXiv:2406.09414*, 2024. 2, 7
- [56] Chongjie Ye, Lingteng Qiu, Xiaodong Gu, Qi Zuo, Yushuang Wu, Zilong Dong, Liefeng Bo, Yuliang Xiu, and Xiaoguang Han. Stablenormal: Reducing diffusion variance for stable and sharp normal. *ACM Transactions on Graphics (TOG)*, 2024. 3
- [57] Yu-Ying Yeh, Zhengqin Li, Yannick Hold-Geoffroy, Rui Zhu, Zexiang Xu, Miloš Hašan, Kalyan Sunkavalli, and Manmohan Chandraker. Photoscene: Photorealistic material and lighting transfer for indoor scenes. In *CVPR*, pages 18562–18571, 2022. 1
- [58] Zheng Zeng, Valentin Deschaintre, Iliyan Georgiev, Yannick Hold-Geoffroy, Yiwei Hu, Fujun Luan, Ling-Qi Yan, and Miloš Hašan. RGB $\leftrightarrow$ X: Image decomposition and synthesis using material-and lighting-aware diffusion models. In *ACM SIGGRAPH 2024 Conference Papers*, pages 1–11, 2024. 1, 2, 3, 4, 5, 6, 8
- [59] Lvmin Zhang, Anyi Rao, and Maneesh Agrawala. Adding conditional control to text-to-image diffusion models. In *ICCV*, pages 3836–3847, 2023. 4
- [60] Qing Zhang, Jin Zhou, Lei Zhu, Wei Sun, Chunxia Xiao, and Wei-Shi Zheng. Unsupervised intrinsic image decomposition using internal self-similarity cues. *IEEE Transactions on Pattern Analysis and Machine Intelligence*, 44(12):9669–9686, 2021. 2
- [61] Jingsen Zhu, Fujun Luan, Yuchi Huo, Zihao Lin, Zhihua Zhong, Dianbing Xi, Rui Wang, Hujun Bao, Jiaxiang Zheng,

and Rui Tang. Learning-based inverse rendering of complex indoor scenes with differentiable monte carlo raytracing. In *SIGGRAPH Asia 2022 Conference Papers*, pages 1–8, 2022. [1](#), [2](#), [4](#), [5](#), [6](#), [7](#), [12](#), [14](#), [15](#), [16](#), [17](#)

- [62] Rui Zhu, Zhengqin Li, Janarbek Matai, Fatih Porikli, and Manmohan Chandraker. Irisformer: Dense vision transformers for single-image inverse rendering in indoor scenes. In *CVPR*, pages 2822–2831, 2022. [2](#), [6](#)

## A. Details of Generative Renderer

Our generative renderer aims to take the scene’s intrinsic properties as input and generate the input image as output. It is fine-tuned from Stable Diffusion v2, with a trainable ControlNet conditioned on 9-channel intrinsic properties (albedo, metallic, roughness, normal, and depth). The model is optimized by the AdamW optimizer with a learning rate of  $1e-4$  and a weight decay rate of  $1e-2$ . Unlike traditional physics-based renderers, our generative renderer does not require environmental lighting as input and can still produce realistic rendered images. Besides, as shown in Figure 11, our generative renderer enables various potential applications, including uncontrollable relighting, material editing, and object removal. Specifically, given the scene’s intrinsic properties, our generative renderer can generate images with lighting conditions different from the original image, although this is uncontrollable since the lighting is represented by Gaussian noise. Additionally, we can manually adjust the albedo color for material editing or remove the target object from the intrinsic properties for object removal.

## B. Details of Reconstruction Loss

Similar to Dreamfusion [46], we first compute the gradient of  $\mathcal{L} = \mu_{\theta}(I) \cdot \text{stop\_gradient}[\mathcal{L}_{rec}]$  with respect to the parameters  $\theta$  of the inverse rendering model, where  $\mu_{\theta}(I)$  denotes the predicted intrinsic property and  $I$  is the input image. Then, the parameters can be updated using an optimizer. The pseudo-code is shown in Figure 12.

## C. Details of Application

In order to achieve controllable lighting editing or object insertion, we provide a solution to optimize the environmental lighting based on the high-quality intrinsic properties predicted by our method. Specifically, similar to [28], we use pre-integrated environment lighting parameterized by Spherical Gaussians (SG) for global illumination, along with 48 SG emission profiles to represent point lights. The SG parameters are then determined by optimizing a L2 loss between the re-rendered output and the input. After fitting, the parameters of the light sources, such as color or intensity, can be adjusted independently to achieve controllable lighting editing. Meanwhile, with the environmental lighting of the scene, we can render an image with the inserted 3D object using the estimated lighting to achieve realistic object insertion.

## D. More Visual Comparison on Synthetic Data

Figures 13, 14, 15, 16, and 17 provide more visual comparison of inverse rendering on the synthetic InteriorVerse dataset [61]. As shown, our method clearly outperforms

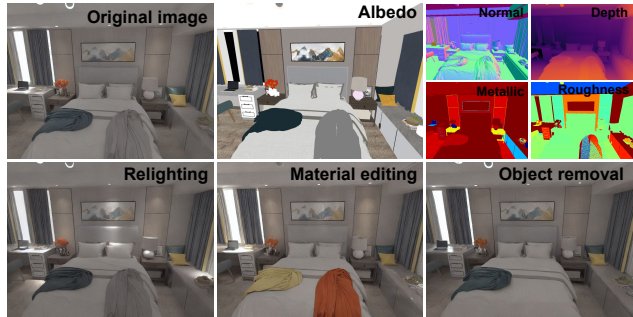


Figure 11. Examples of our generative renderer.

previous methods on material and geometry estimation.

## E. More Visual Comparison on Real Data

Figures 18, 19, 20, 21, and 22 provide more visual comparison on material (albedo, metallic, and roughness) and geometry estimation (depth and normal). Comparing the results, it is clear that our method outperforms current state-of-the-art inverse rendering methods, and is able to produce comparable or even better results than specialized methods for material and geometry estimation.

## F. More Application Results

We in Figure 23 provide more virtual object insertion results, while Figure 24 gives additional results on material and lighting editing. As shown, these application results are visually natural, manifesting the robustness of our predicted intrinsic properties.

```

params = IR_model.init() # inverse rendering model
opt_state = optimizer.init(params)
generative_renderer = diffusion.load_ControlNet()
for nstep in iterations:
    t = random.uniform(0., 1.)
    alpha_t, sigma_t = diffusion.get_coeffs(t)
    eps = random.normal(img_shape) # sample a noise from Gaussian distribution, representing the
    unknown lighting
    intrinsics = IR_model(input_image) # Get an one-step intrinsic properties observation.
    x = input_image
    z_t = alpha_t * x + sigma_t * eps # Diffuse observation.
    epshat_t = generative_renderer.epshat(z_t, intrinsics, t) # Score function evaluation.
    L_rec = epshat_t - eps # generative reconstruction loss
    g = grad(dot(stopgradient[L_rec], intrinsics), params)
    params, opt_state = optimizer.update(g, opt_state) # Update params with optimizer.
return params

```

Figure 12. Pseudo code for the SDS-based reconstruction loss via the generative renderer that defines a differentiable mapping from parameters to intrinsic properties. The gradient  $g$  is computed without backpropagating through the generative renderer’s U-Net. We used the stopgradient operator to express the loss, but the gradient of the parameter can also be easily computed as:  $g = \text{matmul}(L_{rec}, \text{grad}(\text{intrinsics}, \text{params}))$ .

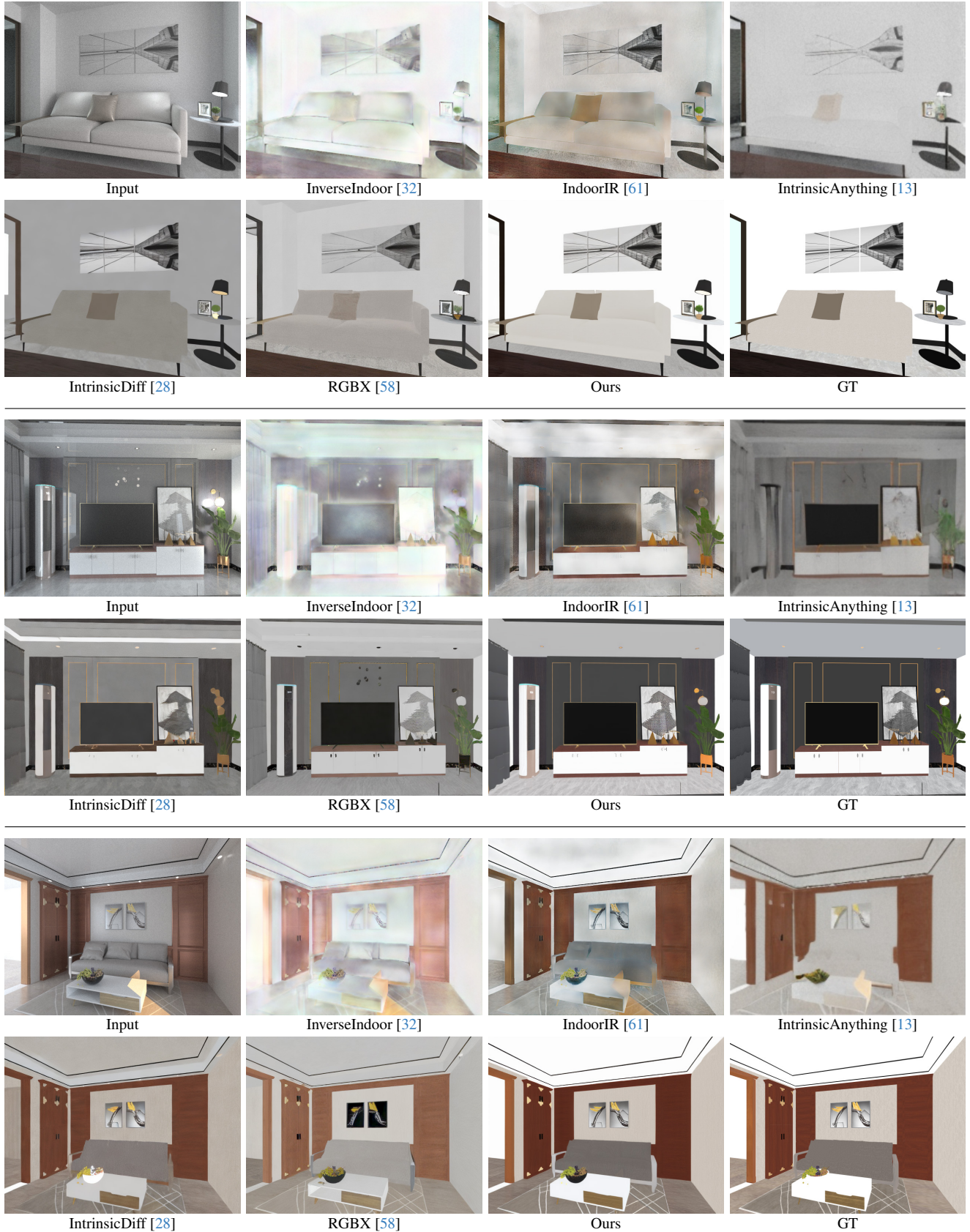


Figure 13. More qualitative comparison of albedo estimation on the synthetic InteriorVerse dataset [61].

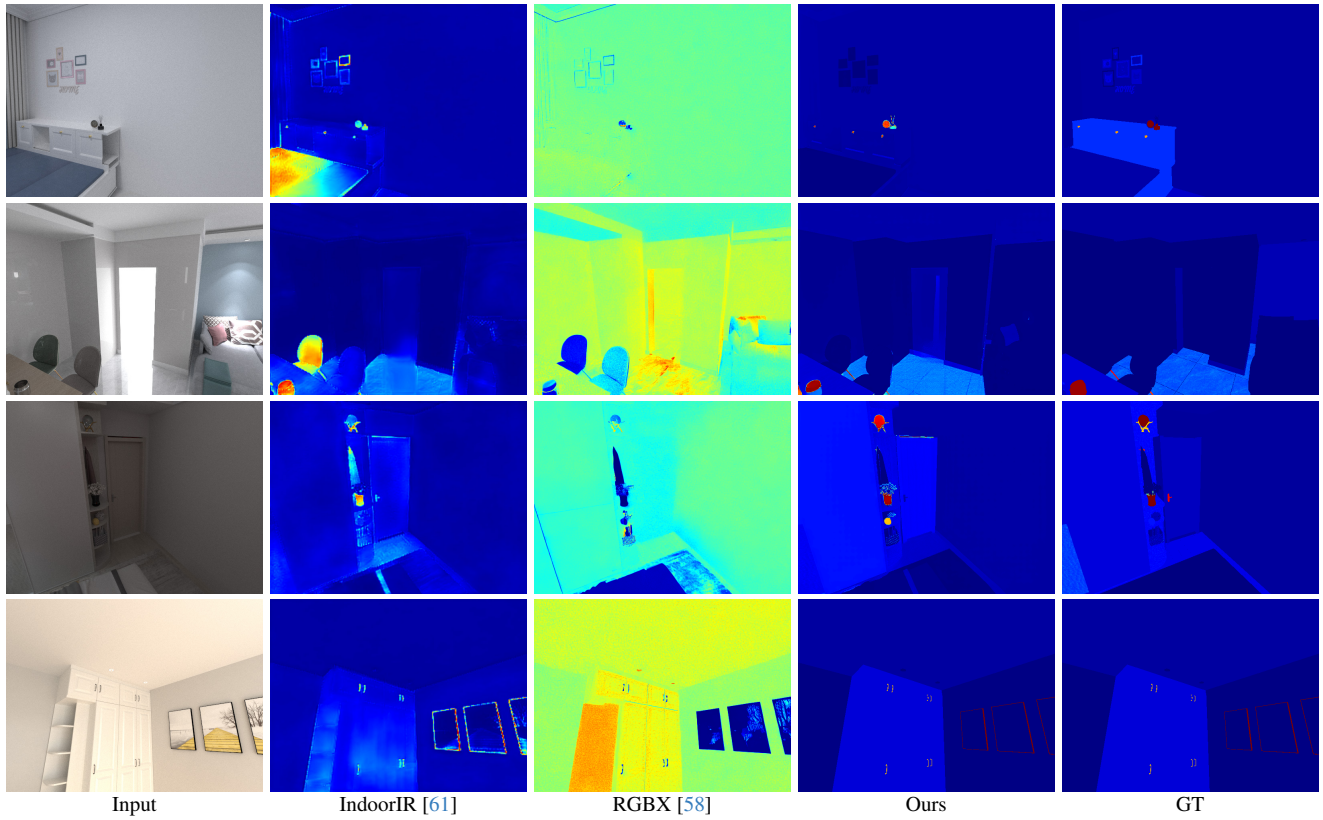


Figure 14. More qualitative comparison of metallic estimation on the synthetic InteriorVerse dataset [61].

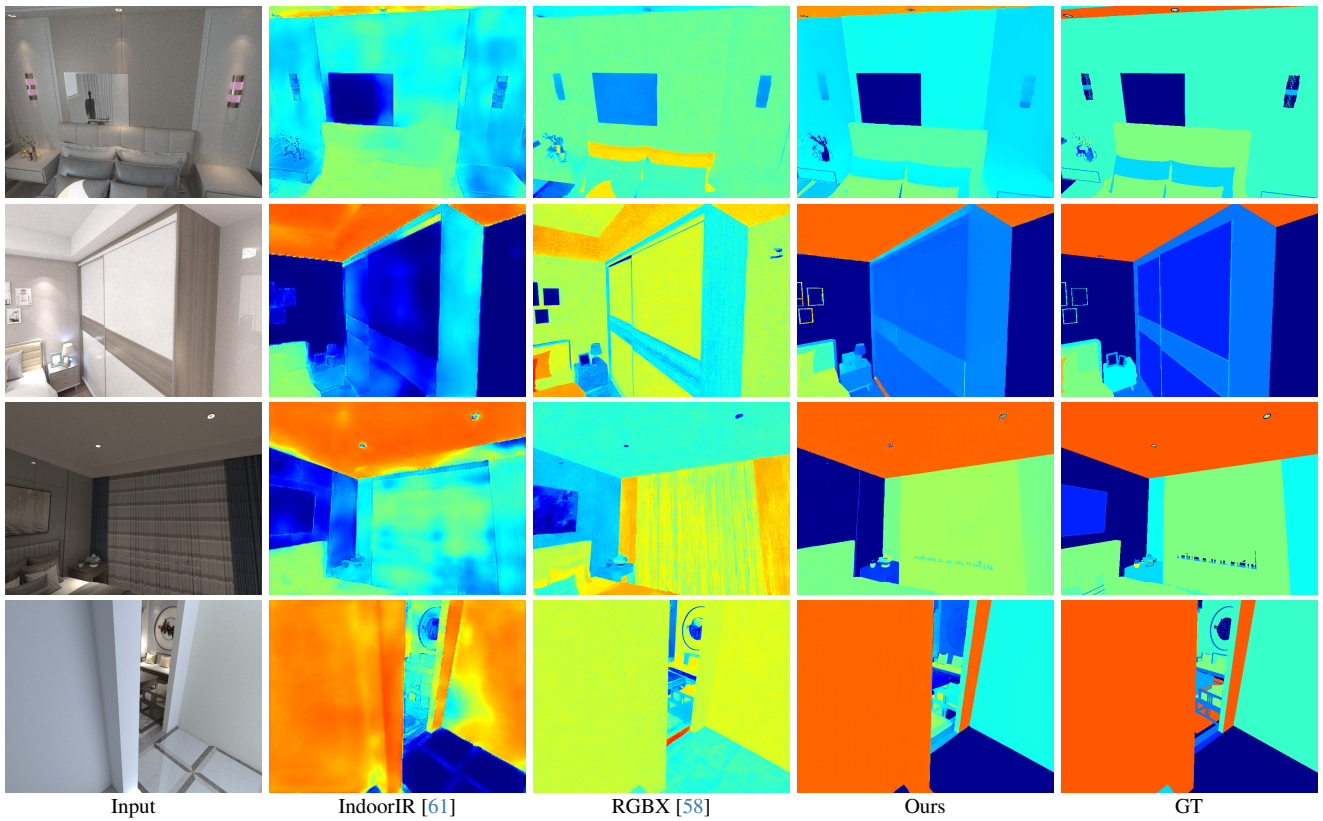


Figure 15. More qualitative comparison of roughness estimation on the synthetic InteriorVerse dataset [61].

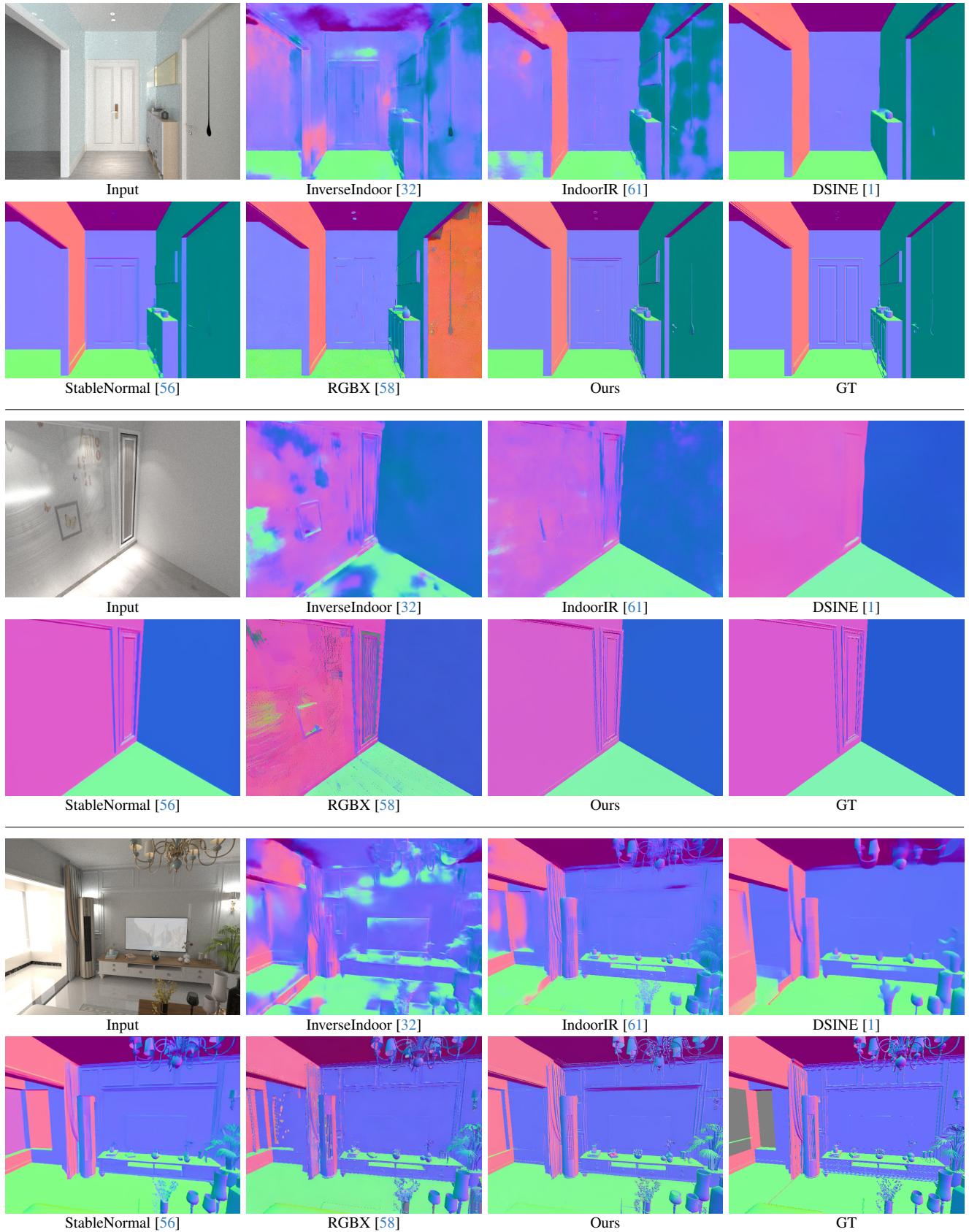


Figure 16. More qualitative comparison of normal estimation on the synthetic InteriorVerse dataset [61].

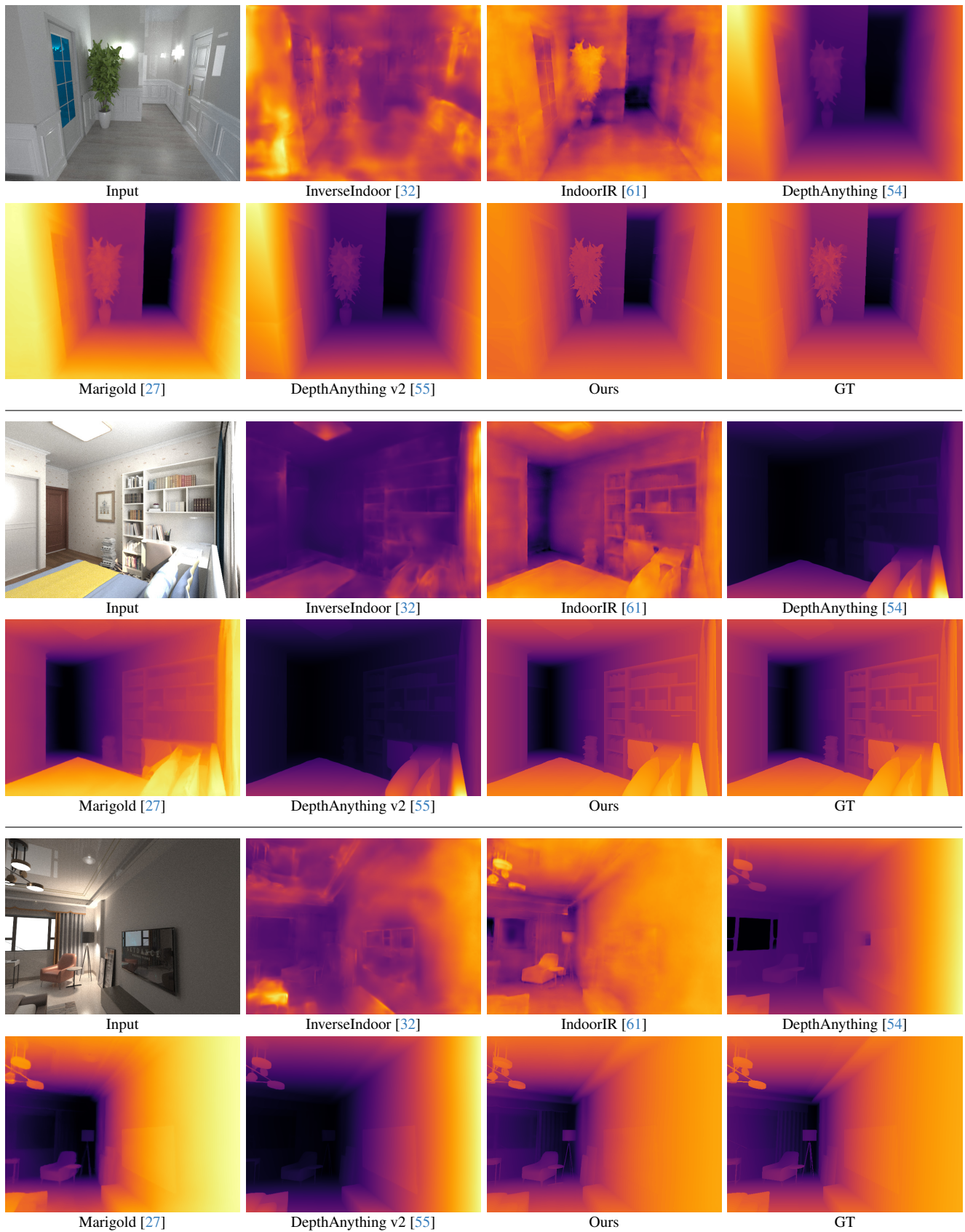


Figure 17. More qualitative comparison of depth estimation on the synthetic InteriorVerse dataset [61].



Figure 18. More qualitative comparison of albedo estimation on real-world images.

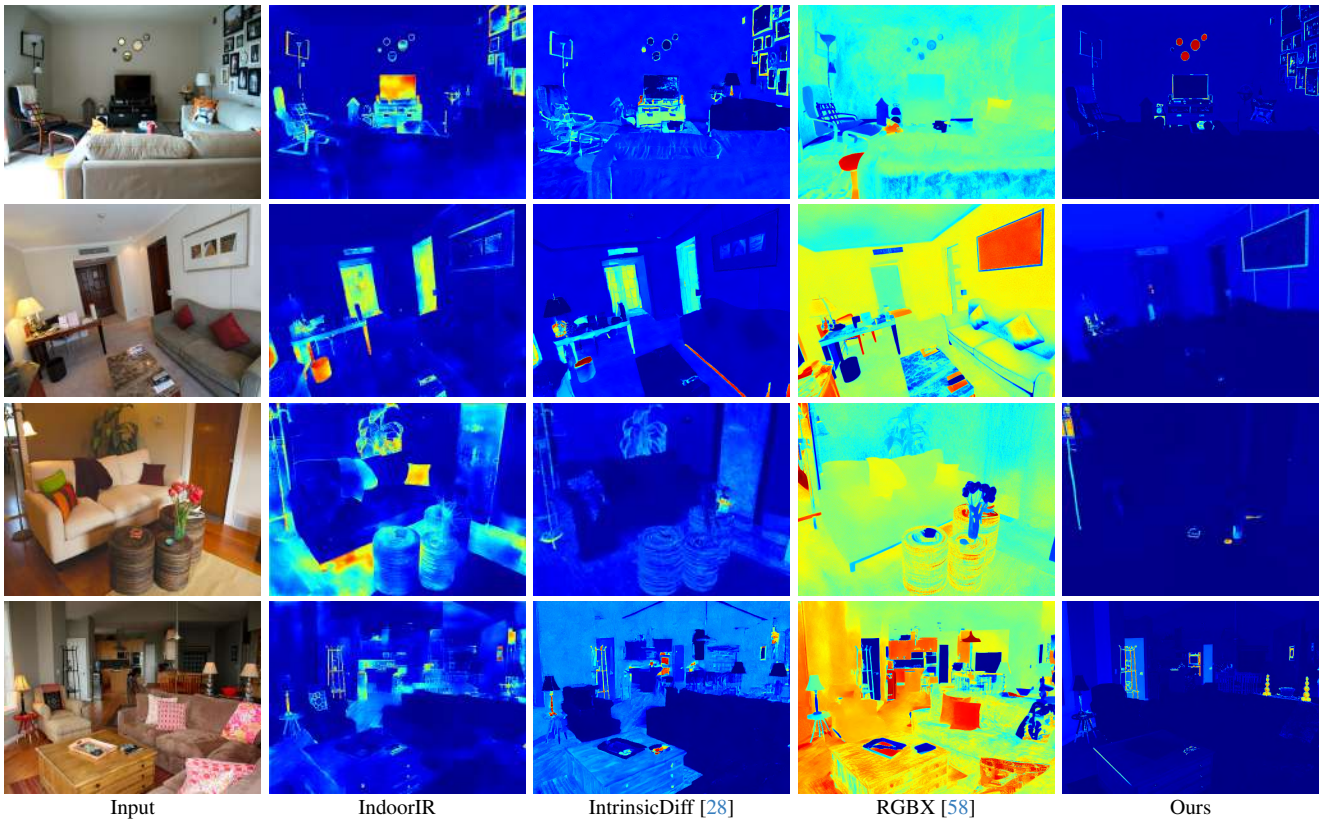


Figure 19. More qualitative comparison of metallic estimation on real-world images.

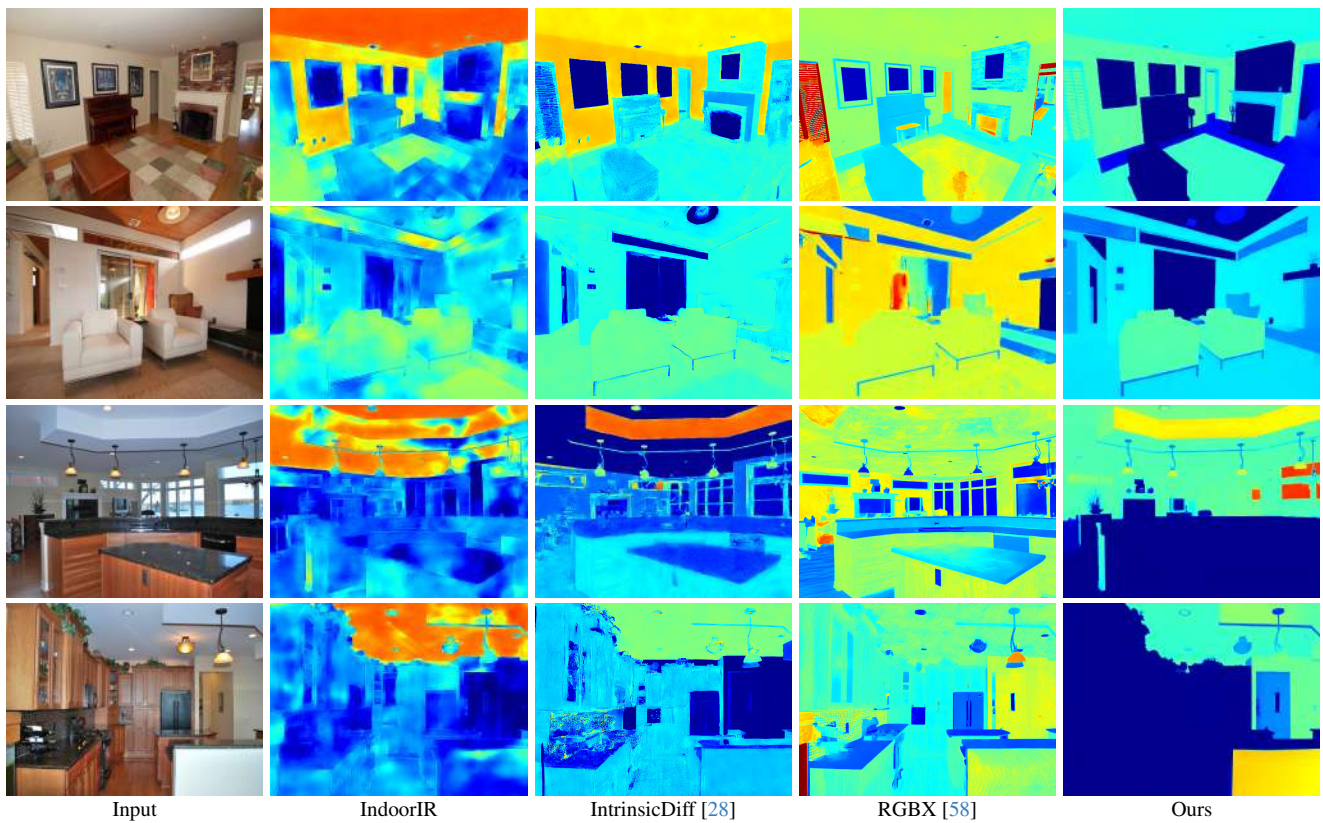


Figure 20. More qualitative comparison of roughness estimation on real-world images.

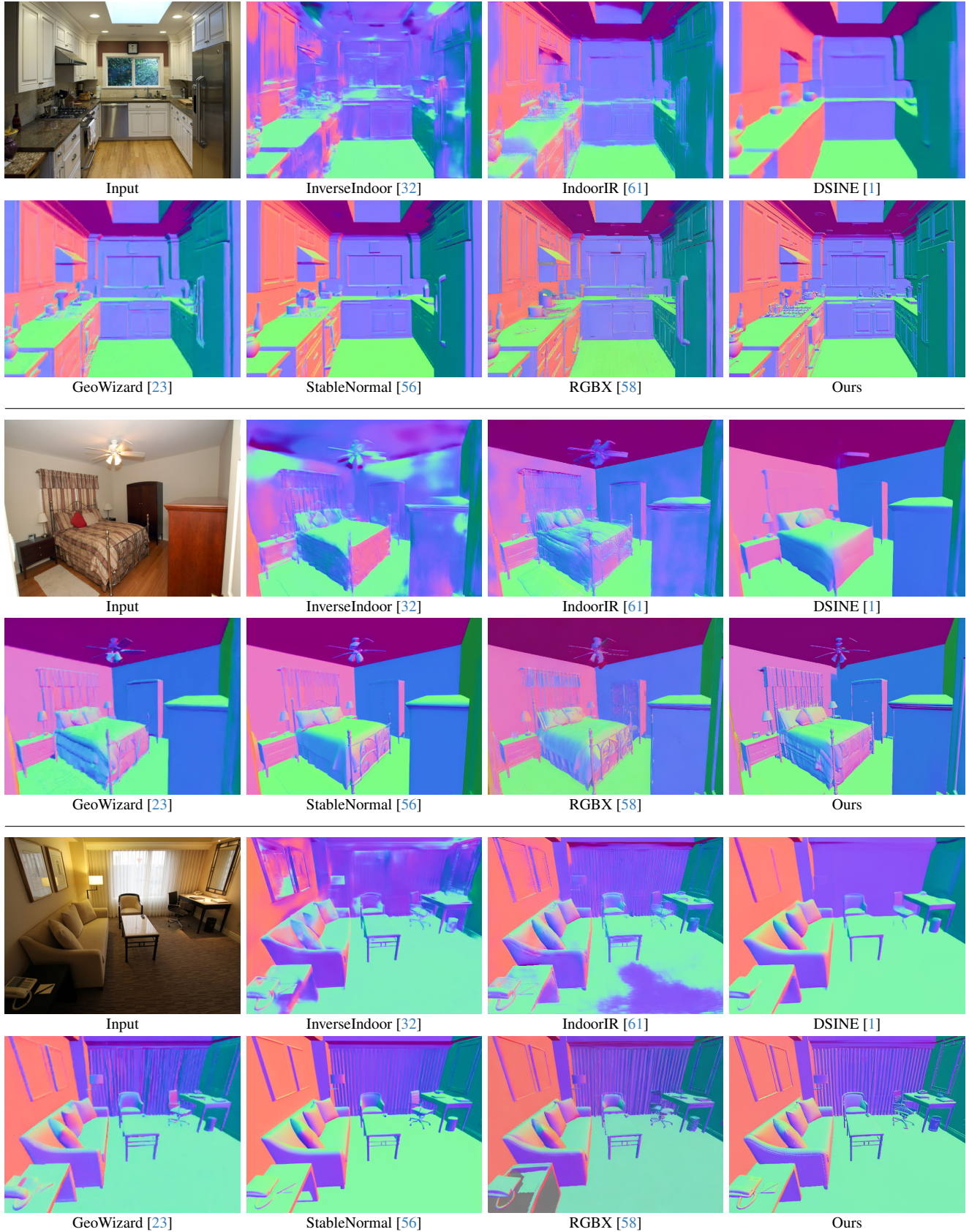


Figure 21. More qualitative comparison of normal estimation on real-world images.

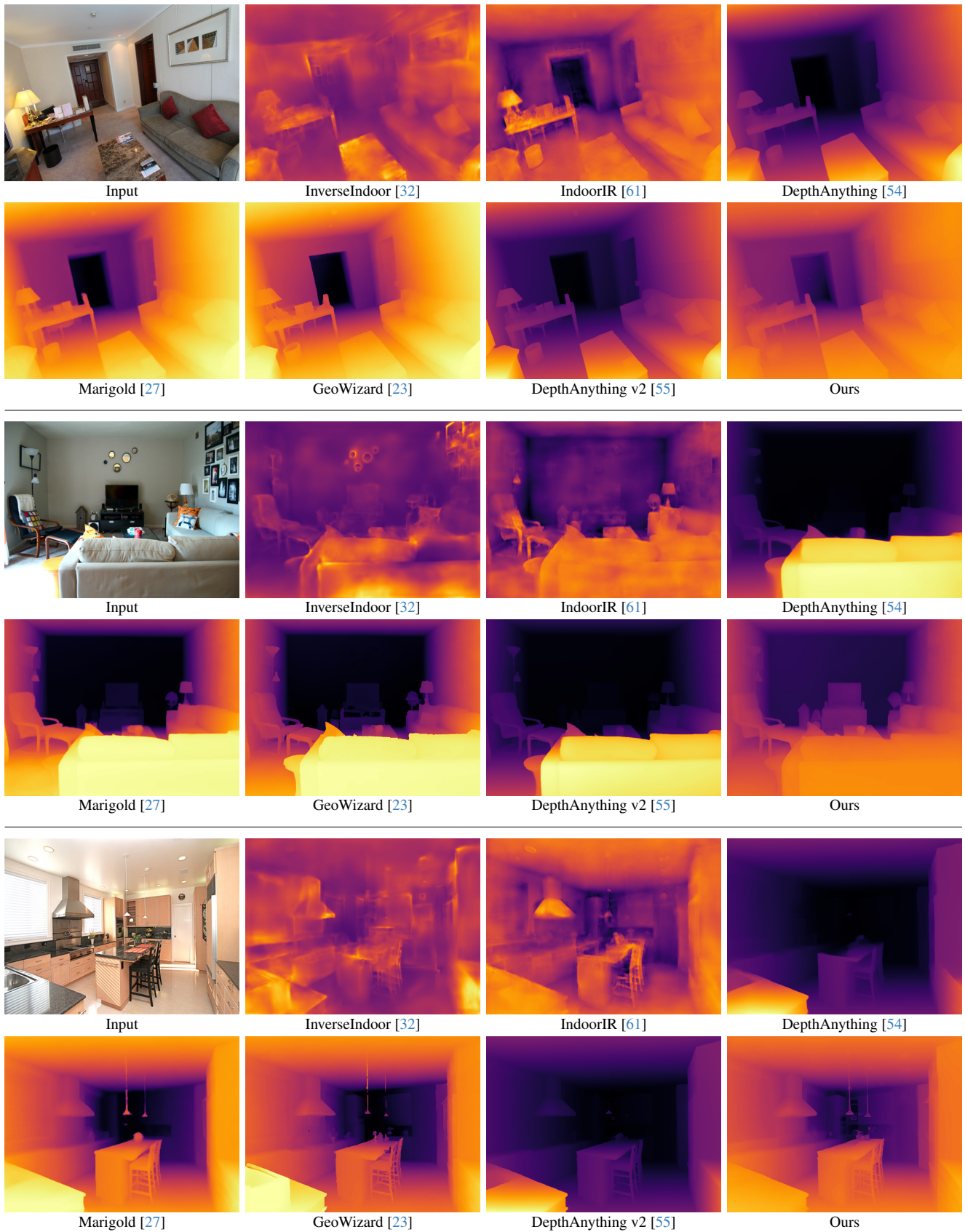


Figure 22. More qualitative comparison of depth estimation on real-world images.

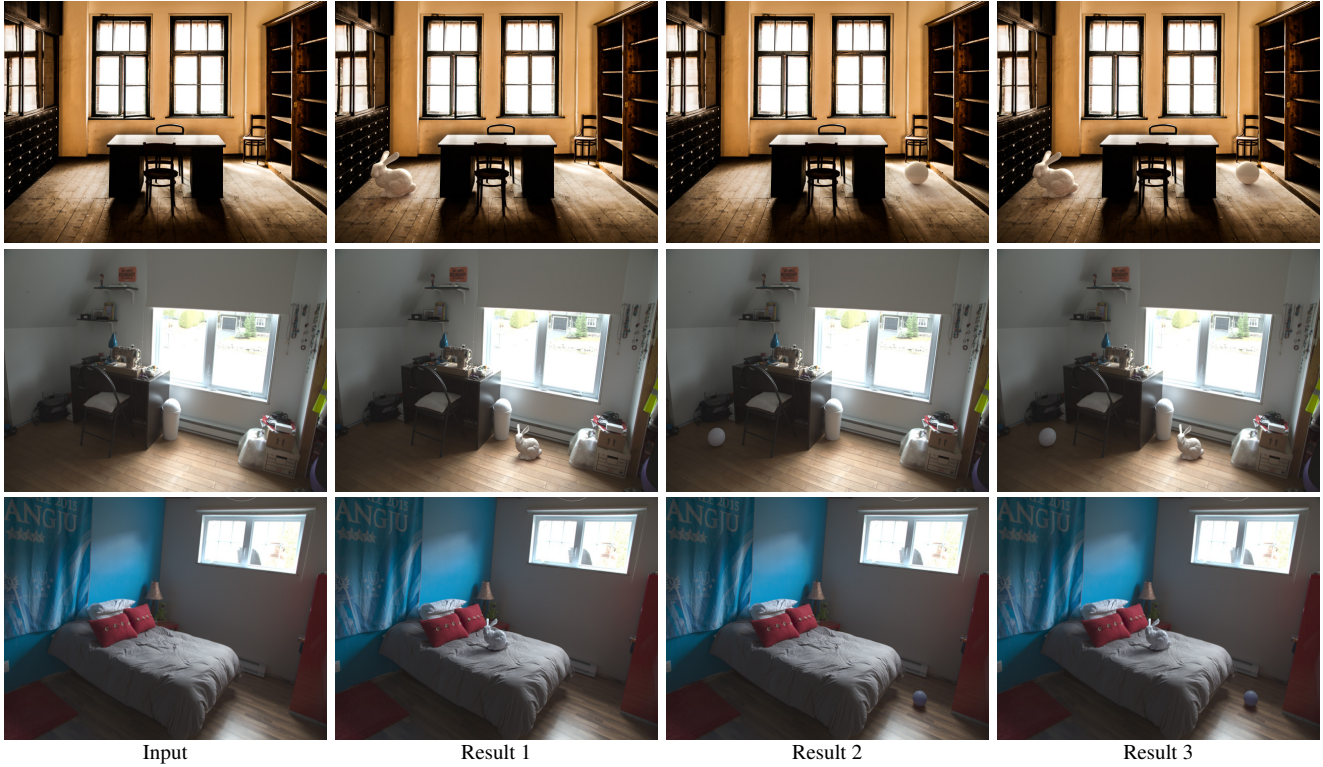


Figure 23. More results of virtual object insertion.

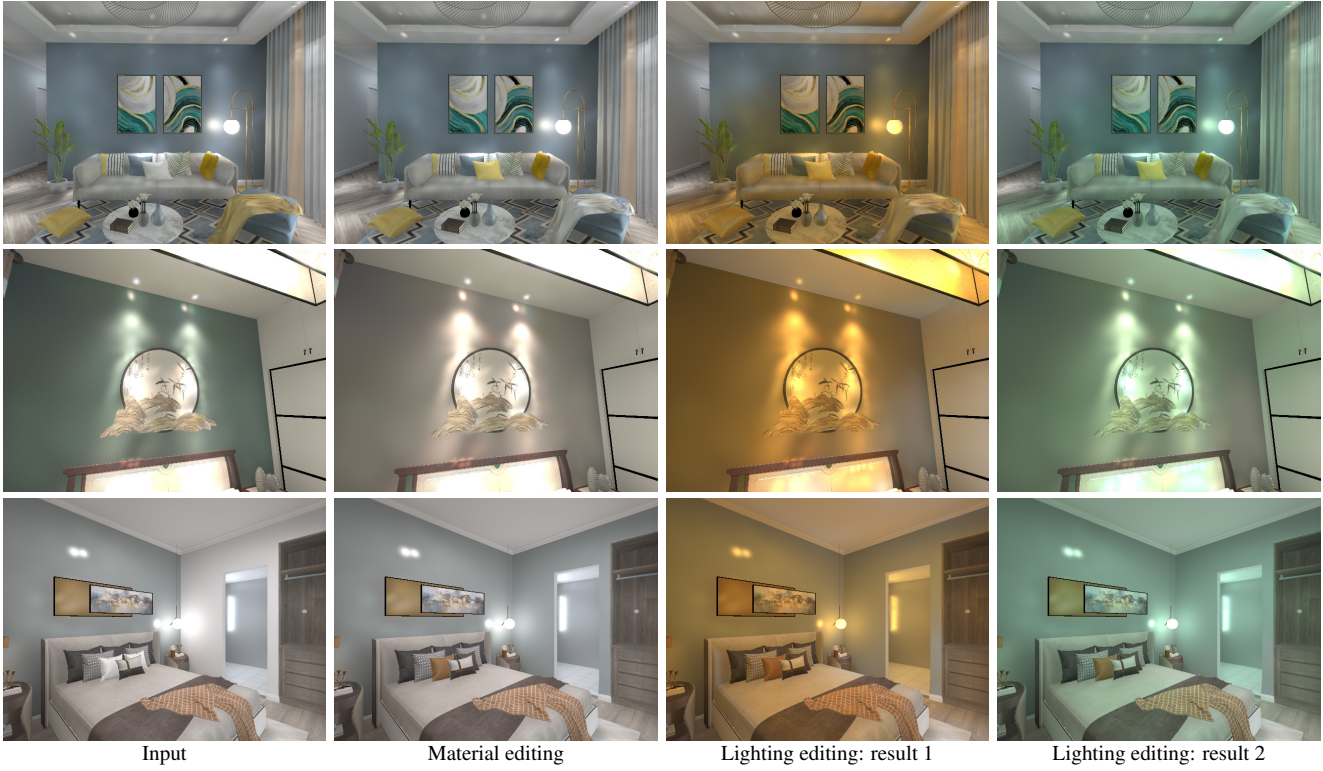


Figure 24. More results of material and lighting editing.